Supporting Information

Fabrication of Conjugated Polymers with Aggregation-Induced Near-Infrared-II Emission for Efficient Phototheranostics

Hui Han, Yuwen Xue, Yafeng Yang, Kai Chen, Pengfei Sun*, Qingming Shen*, Quli Fan *

State Key Laboratory of Organic Electronics and Information Displays & Jiangsu Key Laboratory for Biosensors, Institute of Advanced Materials (IAM), Nanjing University of Posts & Telecommunications, Nanjing 210023, China

E–mail: iampfsun@njupt.edu.cn; iamqmshen@njupt.edu.cn; iamqlfan@njupt.edu.cn.

1. General information and methods

1.1 Materials and animals

4,8–Bis(5–bromo–4–(2–octyldodecyl)thiophen–2–yl)–benzo[1,2–c;4,5–c'] bis [1,2,5] thiadiazole (*m*BT), 4, 8–Bis (5–bromo–3–(2–ethylhexyl)–2–thienyl)–2–benzo [1, 2 – c; 4, 5 – c'] bis [1, 2, 5] thiadiazole (*o*BT), (E)–Butane–2–ene (V), (E) –1, 2–bis (5–methylthiophene–2–yl) ethylene (VT) were purchased from Suzhou Nakai Technology Co., tetrakis (triphenylphosphine) palladium and tris (o–methylphenyl) phosphorus were obtained from J&K Scientific Ltd., pluronic®F–127 were purchased from Shanghai Macklin Biochemical Co. Other chemical catalysts are purchased from commercial sources (such as Aladdin chemical reagent company and Shanghai Macklin Biochemical Co., Ltd, etc.). Among them, toluene was dried and distilled with N2 before use. Unless otherwise indicated, all the synthetic procedures of polymers were performed in an anhydrous and oxygen–free condition, and all original regents except

toluene were directly used. Dulbecco's modified eagle medium (DMEM), fetal bovine serum (PBS), and mouse breast cancer cells (4T1 cells) were achieved from KeyGEN BioTECH.

1.2 Instrumentations Characterization

The ^{1}H NMR spectra were performed on a Bruker Ultra Shield Plus 400 MHz spectrometer at 298 K by choosing $CDCl_3$ as the solvent and tetramethylsilane as the internal standard. The morphology of nanoparticles was observed by a transmission electron microscope (TEM, Hitachi HT7700), whose acceleration voltage is 100 KV. Dynamic light scattering (DLS) analysis was conducted on a commercial laser light scattering spectrometer (ALV–7004; ALV–GmbH, Langen, Germany) equipped with a multi–τ digital time correlator and a He–Ne laser (λ = 632.8 nm). All samples we used for the test were optically cleared by filtration via 0.45 μm Millipore filter. The scattering angle was set up to 90° and all tests were conducted under room temperature. A Shimadzu UV–3600 spectrophotometer was utilized to record the absorption spectra of our samples at room temperature. NIR–II fluorescence spectra were measured using an NIR–II spectrophotometer (Fluorolog 3, Horiba), with an excitation wavelength of 808 nm and 1064 nm obtained from a diode laser operating at 25.0 ± 0.5°C. The 808 nm and 1064 nm laser were purchased from Changchun New Industries Optoelectronics Technology Co., Ltd. The in vitro and in vivo NIR–II FI imaging experiments were conducted on an NIR–II fluorescence imaging system (Wuhan Grand–imaging Technology Co., Ltd) under the 808 nm laser irradiation. A 640 × 512pixel two–dimensional InGaAs array from Princeton Instruments in NIR–II fluorescence windows was equipped in this NIR–II FI system. All photothermal tests were detected using a Fotric 225 instrument (IR thermal camera, ± 2°C) purchased from Fotric Co., Ltd (Shanghai, China). The methyl thiazolyl tetrazolium (MTT) analysis was conducted using a PowerWave XS/XS2 microplate spectrophotometer (BioTek, Winooski, VT). The flow cytometry experiments were performed using a Flow Sight Imaging Flow Cytometer (Novocyte2040R, Aglient, U.S.A). The flow cytometry experiments were performed using a Flow Sight Imaging Flow Cytometer (Merck Millipore, Darmstadt,

Germany). The NIR–II fluorescence imaging experiments were performed by an in vitro and in vivo NIR–II imaging system (Wuhan Grand–imaging Technology Co., Ltd) with 1064 nm LP filters and two types of lenses (50 or 100 mm) under an 808 laser.

1.3 Synthesis of four polymers

1.3.1 Preparation of P*m*BVT, P*m*BV.

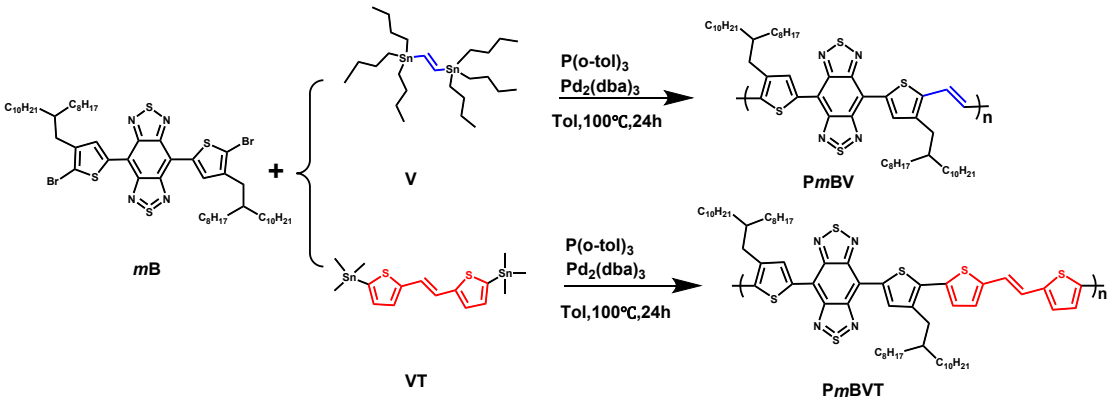

4, 8–Bis(5–bromo–4–(2–octyldodecyl) thiophen–2–yl)–benzo [1, 2 – c; 4, 5 –c'] bis [1, 2, 5] thiadiazole (*m*B, 53.7 mg), (E)–Butane–2–ene (V, 26.0 mg), $Pd_2(dba)_3$ (0.5 mg), $P(o–tol)_3$ (2.0 mg) and anhydrous toluene (2.5 mL) were added into a 10 mL polymerization tube to keep the whole system in an anhydrous and oxygen free environment. Then, it was placed in an oil bath and the temperature was maintained at 90 °C for reaction. When the color of the reaction solution changed from dark green to navy blue, the reaction ended. Cool it to room temperature, extract the reaction solution, settle with methanol, then filter, and finally obtain black solid as the final P*m*BV product. Yield: 70 %.

4, 8–Bis(5–bromo–4–(2–octyldodecyl) thiophen–2–yl)–benzo [1, 2c; 4, 5–c'] bis [1, 2, 5] thiadiazole (*m*B, 53.7 mg), (E)–1, 2–bis(5–methylthiophene–2–yl) ethylene (VT, 30.4 mg), $Pd_2(dba)_3$ (0.5 mg), $P(o–tol)_3$ (2.0 mg) and anhydrous toluene (2.5 mL) were added into a 10 mL polymerization tube to maintain an anhydrous and oxygen free environment for the whole system. Then, they were placed in an oil bath and the temperature was maintained at 100ºC for reaction. When the color of the reaction solution changed from dark green to rufous, the reaction was ended. Cool it to room

temperature, extract the reaction solution, settle with methanol, then filter, and finally obtain dark green solid as the final P*m*BVT product. Yield: 72%.

1.3.2 Preparation of P*o*BVT、P*o*BV.

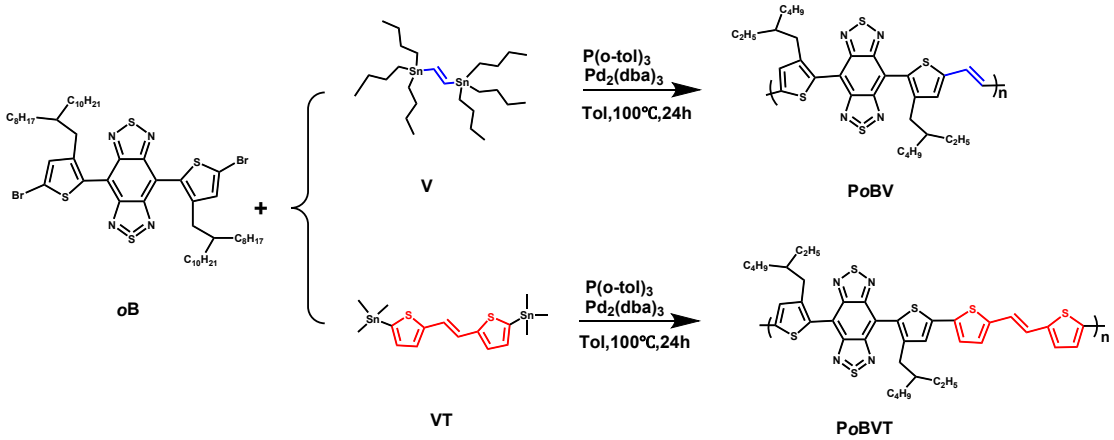

4, 8–Bis(5–bromo–3–(2–ethylhexyl)–2–thienyl)–2–benzo [1, 2–c; 4, 5–c'] bis [1, 2, 5] thiadiazole (*o*B, 36.9 mg), (E)–Butane–2–ene (V, 26.0 mg), P (o– tol)$_3$ (2.0 mg) and anhydrous toluene (2.5 mL) were added into a 10 mL polymerization tube to keep the whole system in an anhydrous and oxygen free environment. Then, it was placed in an oil bath and the temperature was maintained at 100°C for reaction. When the color of the reaction solution changed from dark green to light green, the reaction ended. Cool it to room temperature, extract the reaction solution, settle with methanol, then filter, and finally obtain black solid as the final P*o*BV product. Yield: 76%.

4, 8–Bis(5–bromo–3–(2–ethylhexyl)–2–thienyl)–2–benzo [1, 2–c; 4, 5–c'] bis [1, 2, 5] thiadiazole (*o*B, 36.9 mg), (E)–1, 2–bis(5–methylthiophene–2–yl) ethylene (VT, 30.4 mg), $Pd_2(dba)_3$ (0.5 mg), P(o–tol)$_3$ (2.0 mg) and anhydrous toluene (2.5 mL) were added into a 10 ml polymerization tube to maintain an anhydrous and oxygen free environment for the whole system. Then, they were placed in an oil bath and the temperature was maintained at 100°C for reaction. When the color of the reaction solution changed from dark green to yellow green, the reaction was ended. Cool it to room temperature, extract the reaction solution, settle with methanol, then filter, and finally obtain dark green solid as the final P*m*BVT product. Yield: 73%.

1.4 General Preparation of Nanoparticles.

Sample molecule (such as 1.0 mg P*m*BV) in THF (1.0 mL) was quickly added into deionized water (8.0 mL) containing pluronic®F–127 (12 mg) under continuous ultrasonic dispersion for 10 min. Then, THF was removed by blowing nitrogen gas on the surface of the solution and the purified water–soluble nanoparticles were achieved.

1.5 Determination of quantum yield (QY) of Nanoparticles.

The QY of the dyes was measured in a similar way to the previous report [1], using NIR–II fluorescent IR–26 dye as the reference (QY = 0.5%). For reference calibration, IR–26 dissolved in 1, 2–dichloroethane (DCE) was diluted to a DCE solution to prepare five samples with their absorbance value at 808 nm of ~0.1, ~0.08, ~0.06, ~0.04, and ~0.02. The PL spectra were collected from 850 nm to reject the excitation light (808 nm). Then the emission spectra were integrated in the 1000~1400 nm NIR-II region. The same procedures were performed for the nanoparticles of P*o*BVT and P*o*BV in water. The integrated NIR–II fluorescence intensity was plotted against absorbance at the excitation wavelength of 808 nm and fitted into a linear function. The QY calculation equationwas as follows:

$$QY_{sample} = QY_{ref} \cdot \frac{S_{sample}}{S_{ref}} \cdot \left(\frac{n_{sample}}{n_{ref}}\right)^2 \quad (1)$$

where QY_{sample} is the QY of the nanoparticles in 1000–1400 nm, QY_{ref} is the QY of IR–26 (0.5% in dichloroethane), S_{sample} and S_{ref} refer to the slopes obtained by linear fitting of the integrated emission spectra of the nanoparticles (1000–1400 nm) and IR–26 (1000–1400 nm) against the absorbance at 808 nm, n_{sample} and n_{ref} are the refractive indices of water and DCE, respectively.

1.6 In vitro photothermal effect and photothermal conversion efficiency.

To evaluate the photothermal effect of the P*o*BVT NPs and P*o*BV NPs, 200 μL of three nanoparticle solutions with concentrations of 0.1, 0.08, 0.06 ,0.04 and 0.02 mg mL^{-1} were successively irradiated with 808 nm laser (1.0 W cm^{-2}, 5 min). The temperature changes of the two nanoparticle solutions were performed with an IR thermal camera, and these data were recorded every 30 s.

As we all known, the nature of photothermal therapy is that photothermal agents having the inherent ability to absorb NIR light convert NIR laser energy into heat. Hence, it is important to first explore the photothermal conversion efficiency (ŋ) of the NPs. To study the photothermal conversion behavior of P*o*BVT NPs and P*o*BV NPs, a thermal imaging camera (Fotric 225, Fotric Precision Instruments, USA, ± 2°C) was used to perform the thermal imaging of NPs S7 in an aqueous solution. First, an aqueous solution of nanoparticles (0.1 mg mL^{-1}) was configured, 200 μL of which was added into a 200 μL centrifuge tube. The temperature changes of a fixed concentration of NPs (0.1 mg mL^{-1}) were irradiated with an 808 nm laser (1.0 W cm^{-2}, 5 min), and then the laser was shut off. Finally, we can obtain a temperature increase and drop curve. The photothermal conversion efficiency (η) was calculated using equations (2) and (3) expressed below. The photothermal conversion efficiency of the P*o*BVT NPs and P*o*BV NPs were determined to be through the collected data and equation. [2]

$$\eta = \left[hS(T_{max} - T_{suur}) - Q_{dis}\right] / \left[I(1 - 10^{-A808})\right] \quad (2)$$

$$\tau_s = m_D C_D / hS \quad (3)$$

The parameters S, h, T_{max}, T_{surr}, Q_{dis}, I and A_{808} are the container's surface area, heat–transfer coefficient, maximum laser–trigger temperature, indoor temperature, heat dissipation caused by the light absorbing of quartz cuvette, intensity of laser (1.0 W cm^{-2}) and absorbance of P*o*BVT NPs and P*o*BV NPs at 808 nm, respectively.

Parameter τs is the time constant of the sample system. The parameters m_D and C_D are the mass and heat capacity of the solvent, respectively.

2. Phototheranostics Assessment In vitro and in vivo

2.1 In vitro Photocytotoxity Assay

The 4T1 cells were used for the in vitro cytotoxicity assessment of P*o*BVT NPs by MTT assays. First, cells, seeded at 2×10^4 cells/well, were cultured in DMEM in 96–well plates at 37 °C and 5% CO_2 condition for 24 h. Then, the medium was replaced by

a mixture of fresh DMEM medium and different concentrations of P*o*BVT NPs (0, 12.5, 25, 50, 100 and 200 μg mL^{-1}), following which the selected wells (P*o*BVT NPs + laser group) was irradiated under 808 nm laser illumination (1.0 W cm^{-2}) for 5 min and further incubated at 37 °C and 5% CO_2 for 24 h. The P*o*BVT NPs treated wells (P*o*BTV NPs group) was not irradiated with 808 nm laser illumination. Afterwards, the medium was replaced with 100 μL of fresh DMEM medium, and 20 μL of MTT (5.0 mg mL^{-1}) was added to each well. Finally, after 4 h of incubation, the upper supernatant was removed, and 100 μL of DMSO was added. Cell viability was calculated by measuring the absorbance at 490 nm using a Power Wave XS/XS2 microplate spectrophotometer.

2.1 Assessment of NIR–II PTT in vitro by Confocal Imaging and Flow Cytometry

The 4T1 cells were used for the assessment of the photothermal effect by confocal imaging. Firstly, the 4T1 cells were cultured with DMEM in CLSM culture dishes (Costar) until the cell density increased to 1×10^5 cells mL^{-1} per well. Subsequently, the medium was replaced with a S9 mixture medium (100 μg mL^{-1}) of the fresh DMEM medium and P*o*BVT NPs for 12 h in the dark, the media were removed, the cells were washed by PBS and replaced with fresh DMEM. The selected wells were then irradiated with or without the 808 nm laser illumination (1.0 W cm^{-2}, 5 min), respectively. After 24 h of apoptosis, the cells were washed twice to remove the cell debris and were then incubated with calcein– AM/propidium iodide (PI) dye solution for 10 min. Finally, the cells were imaged using CLSM (Olympus Fluoview FV1000, Olympus Corp., Japan). The 4T1 cells were used for the assessment of the photothermal effect by flow cytometry. First, the 4T1 cells were cultured with DMEM in 6–well plates until the cell density increased to 1×10^5 cells mL^{-1} per well. The medium was then replaced with a mixture medium of fresh DMEM medium and P*o*BVT NPs (100 μg mL^{-1}) for 12 h in the dark, the media were removed, the cells were washed by PBS and replaced with fresh DMEM. Subsequently, the selected wells were irradiated with or without the 808 nm laser illumination (1.0 W cm^{-2}, 5 min), respectively. After 24 h of apoptosis, the wells underwent two iterations of supernatant removal and the 500 μL PBS addition to remove dead cells. The PBS was then removed and EDTA was added, and the cells

were dissolved in an incubator at 37°C and 5% CO_2 condition for 7 min. Later, 1 mL of DMEM was added, and the cells were transferred into a 15 mL centrifuge tube. After the cells were centrifuged for 3 min, the supernatant was removed, Annexin V–FITC/PI dye solution was added to the collected cells for staining, and the cells were tested by Novocyte2040R.

2.2 Animals and tumor models.

4T1 tumor-bearing mice (age 5-6 weeks) were obtained from the Jiangsu KeyGEN BioTECH. All animals were acclimatized to the animal facility for one week prior to experimentation and housed under pathogen free conditions. All animals were fed under conditions of 25°C and 55% of humidity and allowed free access to standard laboratory water and chow. All the animal procedures were performed according to the guidelines of the Animal Ethical and Welfare Committee of Nanjing University of Posts & Telecommunications. 4T1 tumors were planted by hypodermic injection of suspension of 4T1 cells into the right armpit of mice. In vivo NIR–II fluorescence and photothermal imaging. The 4T1 tumor–bearing mice were administered with P*o*BVT NPs in saline at a dose of 200 μg P*o*BVT NPs per mouse via tail vein. Then, at 6, 12, 24, 36 and 48 h post–injection, the mice were anesthetized using 2% isoflurane in oxygen and underwent NIR–II fluorescence imaging through a commercial measurement purchased from Suzhou NIR–Optics Technologies CO., Ltd., with the long pass (LP) filter of 1064 nm. For in vivo photothermal imaging, the infrared thermal images of mice were acquired using an E50 IR camera during the irradiation of 808 nm laser (1.0 W cm^{-2}) for 6 min at 24 h after administration with P*o*BVT NPs. Mouse injected with saline under the same irradiation condition was used as the control.

2.3 In vivo phototherapeutic study.

When the inoculated tumor grew for 8 d, 15 mice were randomly divided into 3 groups, named “PBS”, “P*o*BVT NPs”, and “P*o*BVT NPs + L”, respectively. On day 0, for “PBS” and “P*o*BVT NPs” groups, 200 μL of PBS and P*o*BVT NPs (1.0 mg mL^{-1}) were separately injected into the 4T1 tumor–bearing mice through tail vein without

subsequent laser irradiation. In case of "P*o*BVT NPs + L" groups, after intravenous injection 200 μL of P*o*BVT NPs (1.0 mg mL^{-1} P*o*BVT NPs) for 24 h, respectively, the tumors of mice in each group were continuously irradiated with 808 nm laser (1.0 W cm^{-2}) for 6 min. After a variety of treatments, the mouse body weight and tumor volume were recorded every 3 days during 14–day study duration. The tumor volume was measured by a vernier caliper and calculated as $V = a \times b^2/2$ (a: tumor length; b: tumor width). In addition, the tumor tissues were hen subjected to H&E staining and immunohistochemical studies.

2.4 In vivo toxicity evaluation.

All the mice were sacrificed after complete treatment of 14 days. The major organs (heart, liver, spleen, lung and kidney) were dissected from the mice. After the tissues were fixed in 4% neutral-buffered paraformaldehyde and embedded in paraffin for hematoxylin-eosin (H&E) staining. The sections were then subjected to H&E staining for histopathological evaluation.

2.5 Statistical analysis.

Unless otherwise stated, statistical comparisons between various groups were performed using with one–way analysis of variance (ANOVA) with a corrected p value below 0.05 considered statistically to be significant (*$p < 0.05$, **$p < 0.01$, ***$p < 0.001$). All data were generated from the mean values of three independent experiments and are presented as the mean ± standard deviation (s.d.).

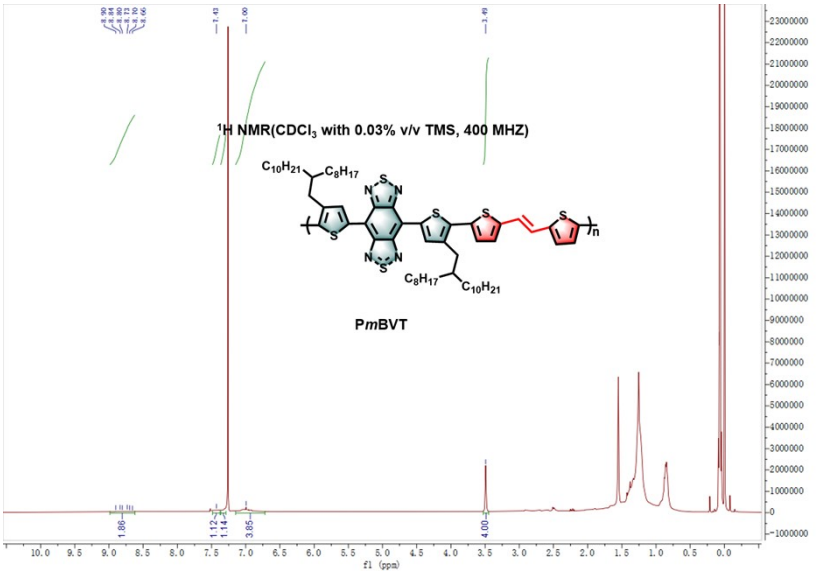

Fig. S1 The ^{1}H NMR spectrum of P*m*BVT.

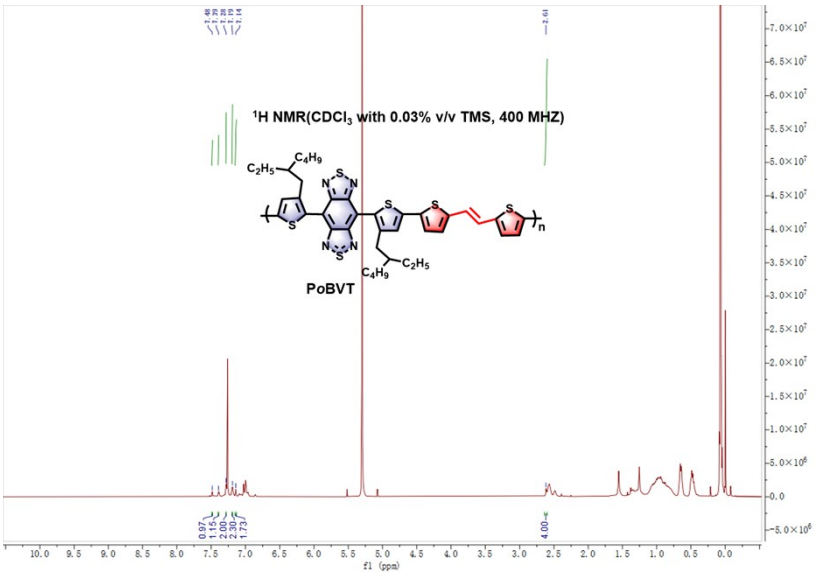

Fig. S2 The ^{1}H NMR spectrum of P*o*BVT.

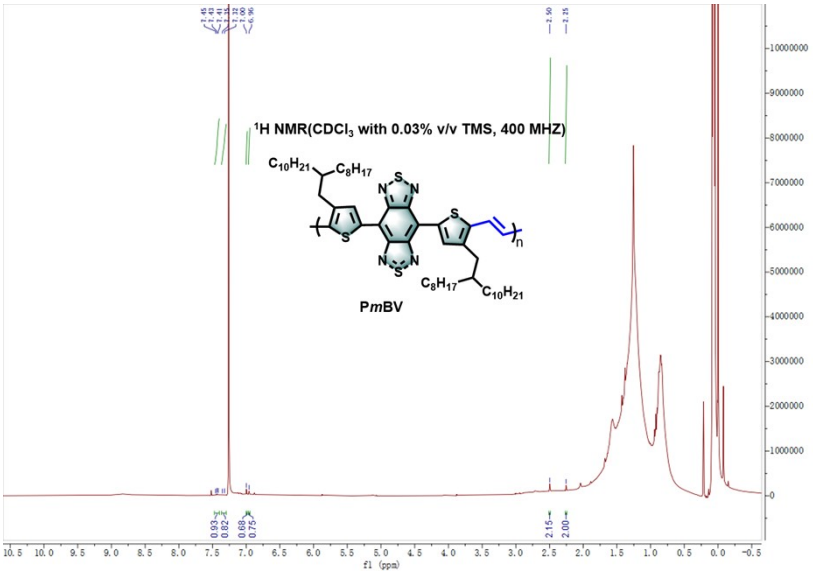

Fig. S3 The ^{1}H NMR spectrum of P*m*BV.

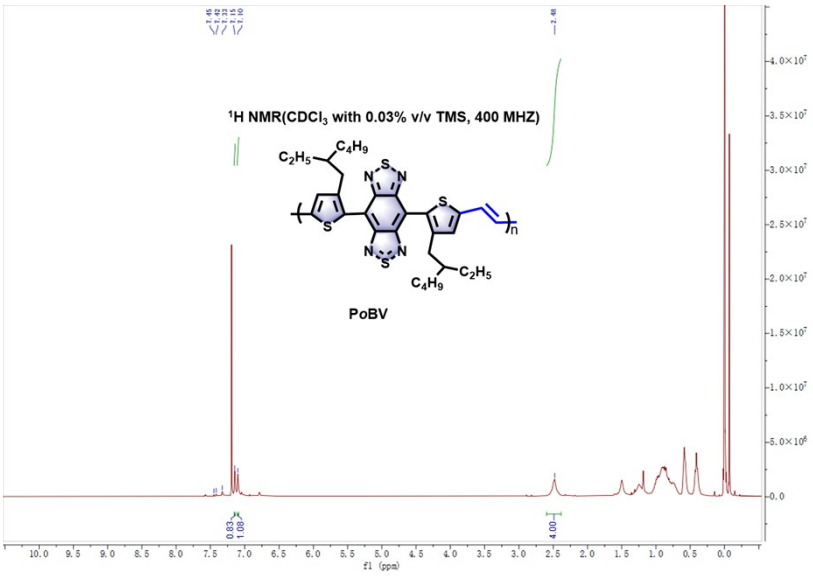

Fig. S4 The ^{1}H NMR spectrum of P*o*BV

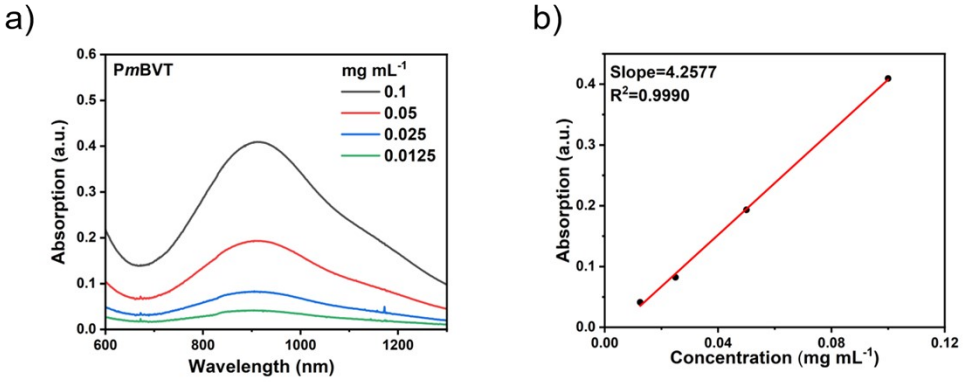

Fig. S5 (a) UV–vis–NIR absorption spectra of P*m*BVT in THF at different concentrations. (b) The mole extinction coefficient of P*m*BVT at 808 nm.

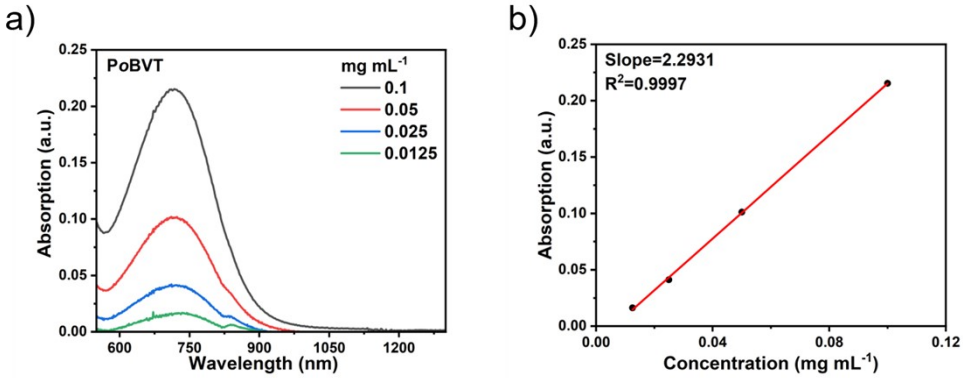

Fig. S6 (a) UV–vis–NIR absorption spectra of P*o*BVT in THF at different concentrations. (b) The mole extinction coefficient of P*o*BVT at 808 nm.

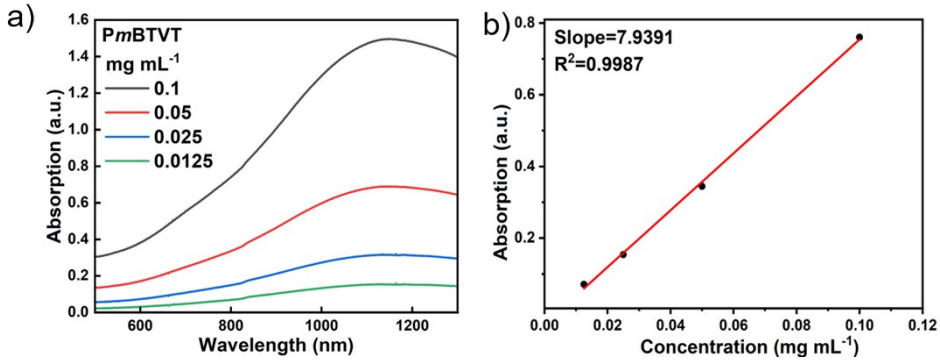

Fig. S7 (a) UV–vis–NIR absorption spectra of P*m*BV in THF at different concentrations. (b) The mole extinction coefficient of P*m*BV at 808 nm.

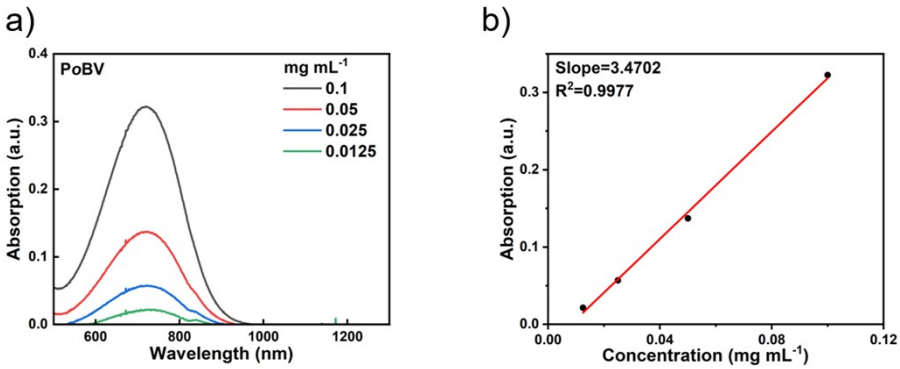

Fig. S8 (a) UV–vis–NIR absorption spectra of P*o*BV in THF at different concentrations. (b) The mole extinction coefficient of P*o*BV at 808 nm.

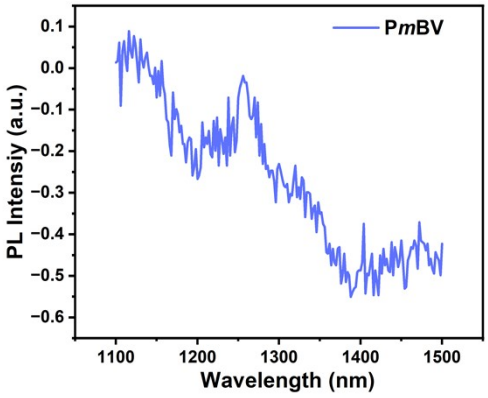

Fig. S9 PL intensity of P*m*BV in THF (0.1 mg mL^{-1}).

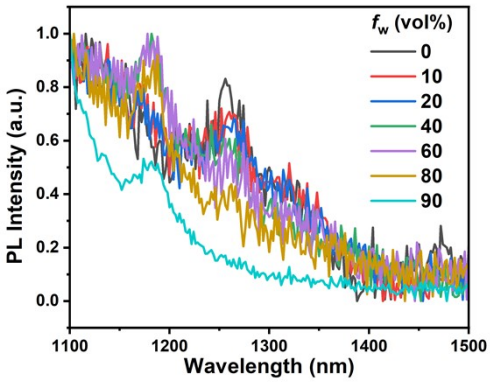

Fig. S10 The NIR-II fluorescence emission spectra of P*m*BV in THF and water mixtures was studied by increasing the water content from 0% to 90% under 1064 nm excitation.

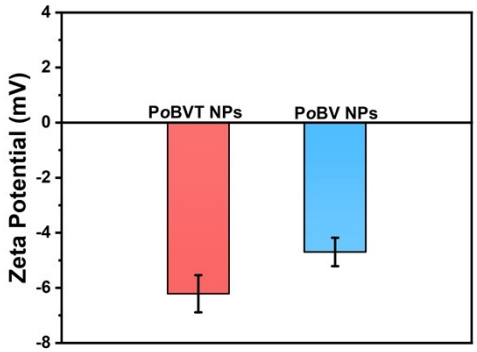

Fig. S11 Zeta potential of PoBVT NPs and PoBV NPs.

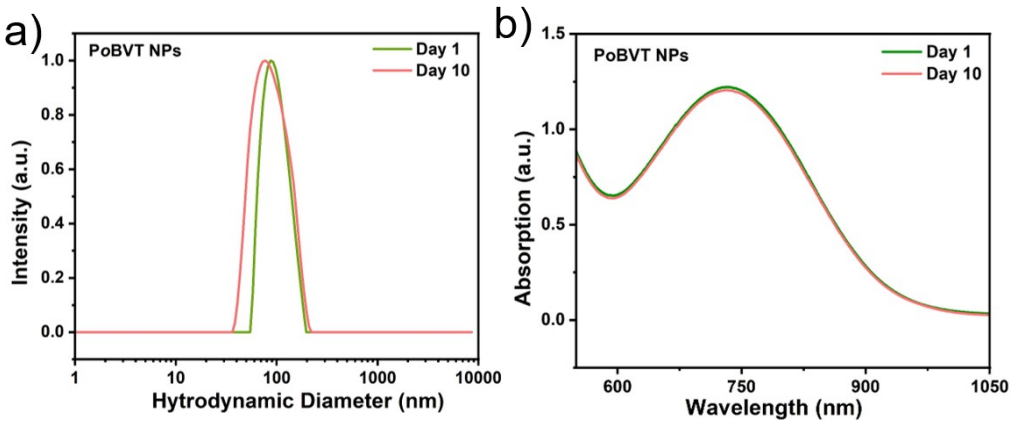

Fig. S12 (a) DLS profile of P*o*BVT NPs in water on the 1th and 10th days, respectively. b) Absorption spectra of P*o*BVT NPs in water with concentration of 0.1 mg mL^{-1}on the 1th and 10th days, respectively.

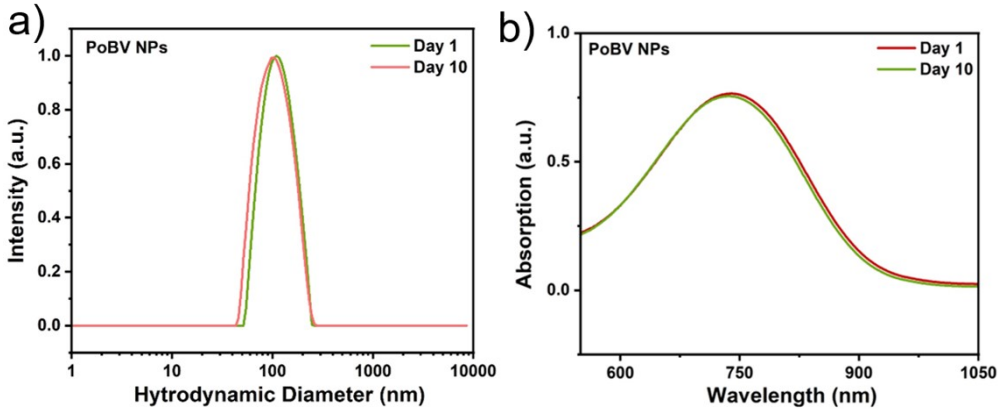

Fig. S13 (a) DLS profile of P*o*BV NPs in water on the 1th and 10th days, respectively. b) Absorption spectra of P*o*BV NPs in water with concentration of 0.1 mg mL^{-1}on the 1th and 10th days, respectively.

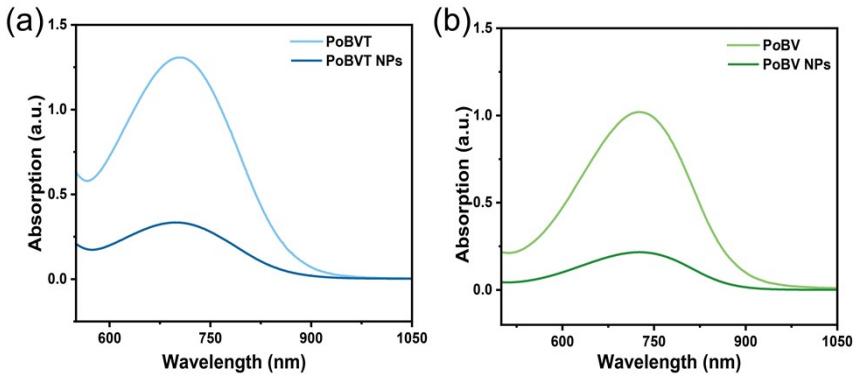

Fig. S14 Ultraviolet spectrophotometry was used to determine the encapsulation efficiency of PoBVT NPs and PoBV NPs.

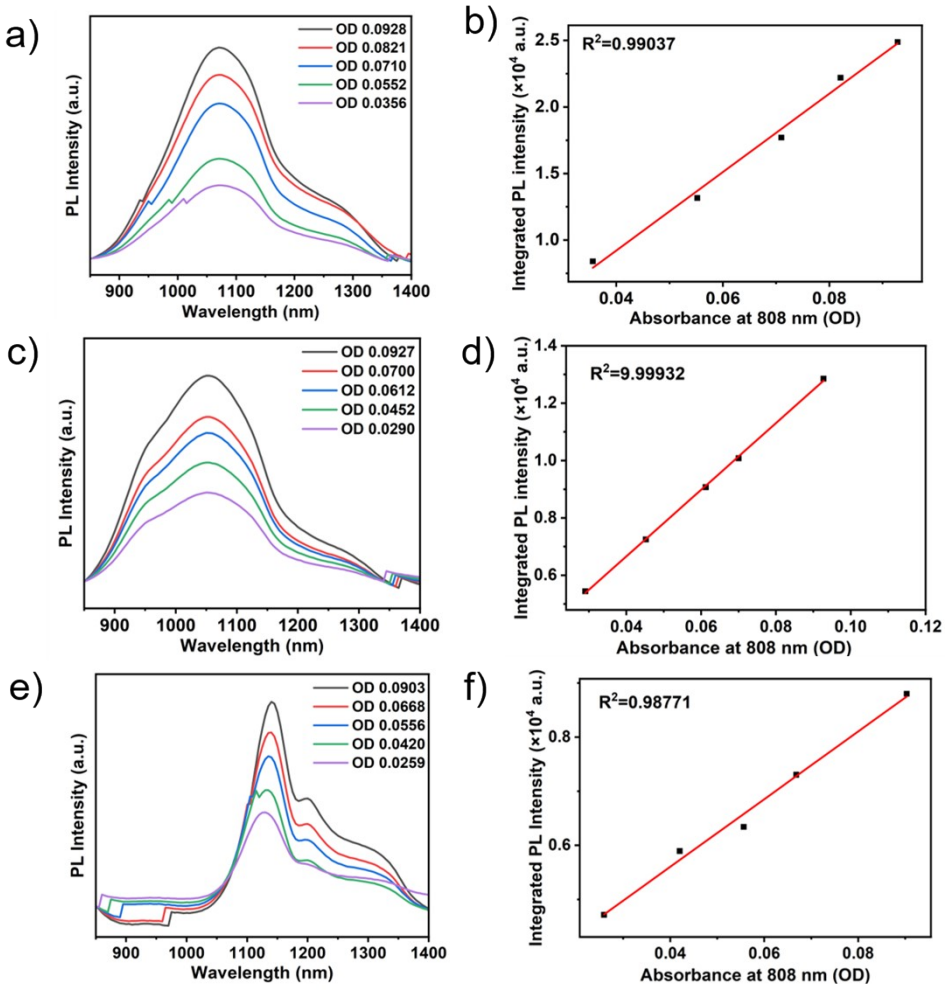

Fig. S15 NIR–II quantum yield measurement of nanoparticles. PL spectra and a plot of integrated fluorescence intensity NIR–II (1000~1400 nm) vs the absorbance at 808 nm of (a, b) P*o*BVT NPs in ultrapure water, (c, d) P*o*BV NPs in ultrapure water and (e, f) IR–26 in DCE solution.

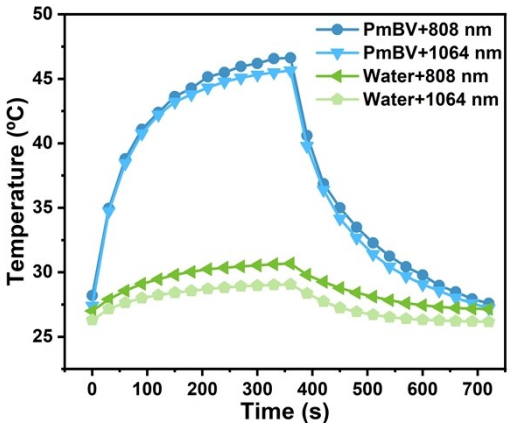

Fig. S16 The photothermal behavior of water, PmBV NPs, which was irradiated with 808 nm (1.0 w cm^{-2}) and 1064 nm (1.0 w cm^{-2}) light for 6 min, then the laser was removed, and the samples were naturally cooling down.

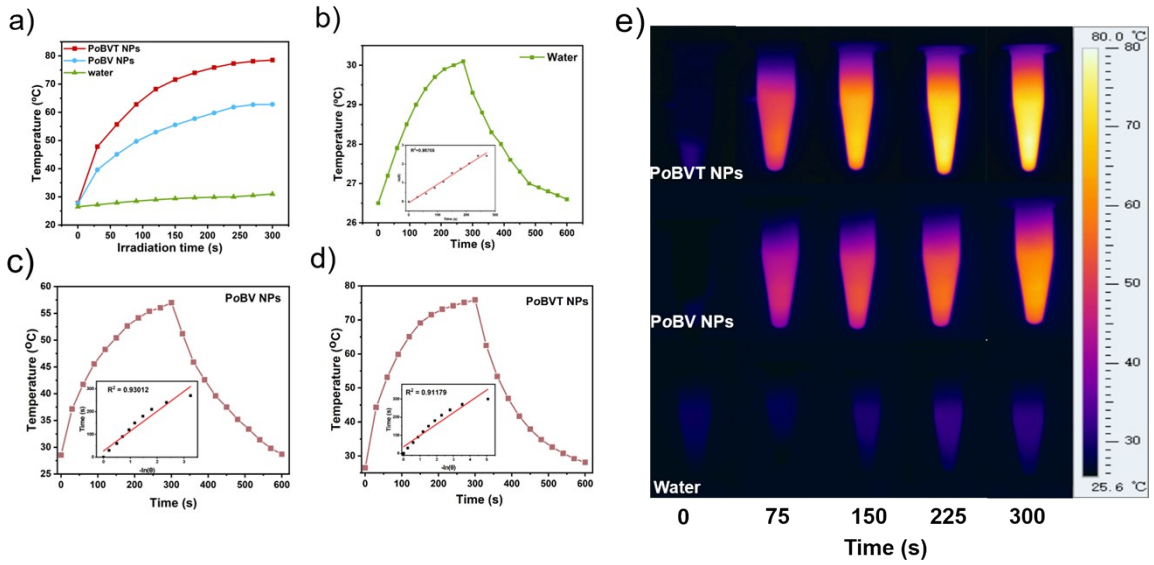

Fig. S17 (a) Photothermal performances of P*o*BVT NPs and P*o*BV NPs (100 μg mL^{-1}) under 808 nm irradiation (1.0 W cm^{-2}). (b–d) The photothermal behavior of water, P*o*BVT NPs and P*o*BV NPs, which were irradiated with 808 nm light for 5 min, then the laser was removed, and the samples were naturally cooling down. Inset: Plots of irradiation time versus –ln(θ) for P*o*BVT NPs and P*o*BV NPs. The slope indicates its system time constant (τs). (e) The corresponding infrared thermal pictures.

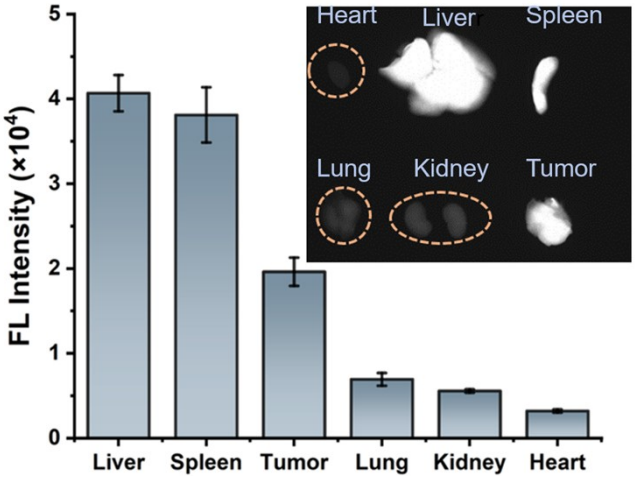

Fig. S18 (a) In vitro NIR–II fluorescence images of tumor and major organs (heart, liver, spleen, lung, and kidney) after 48 h of intravenous injection (808 nm laser, 1064 nm LP filter, 200 ms). (b) Quantitative NIR-II fluorescence intensity of tumor and major organs.

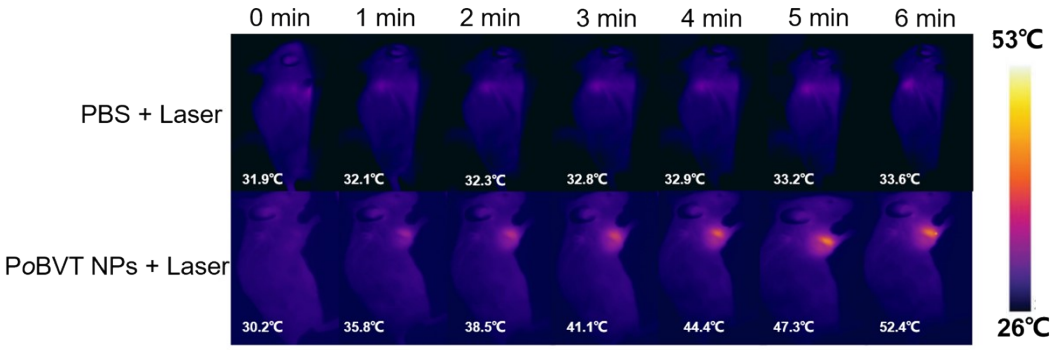

Fig. S19 photothermal imaging results of the 4T1 tumor-bearing mice after treatment with P*o*BVT NPs via the tail intravenous administration method at different detecting times.

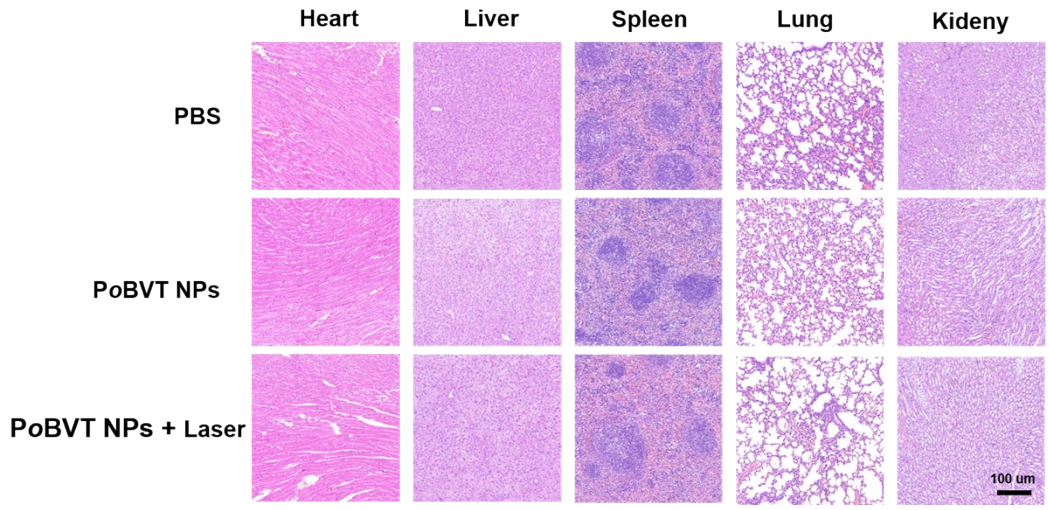

Fig. S20 H&E staining images of organs (heart, liver, spleen, lung, and kidney) sections obtained from the five treatment groups.

Table S1. Optical properties of conjugated polymers.

Dye in THF	**P*o*BVT**	**P*o*BV**	**P*m*BVT**	**P*m*BV**
λ_{abs} (nm)	725	726	925	1139
λ_{em} (nm)	1080	1048	1115	–
Stoke shift (nm)	355	322	190	–
$\varepsilon_{max,\ 808nm}$ (10^3 M^{-1} cm^{-1})	2.29	3.47	4.26	7.92
α_{AIE}	3.46	1.55	0.02	0.66

3. References

[1] D. Yan, W. Xie, J. Zhang, L. Wang, D. Wang, B. Z. Tang, *Angew. Chem. Int. Ed.* **2021**, 60, 26769–26776.

[2] C. Xu, K. Pu, *Chem. Soc. Rev.* **2021,** *50*, 1111–1137.